Biochemical Alterations from Normal Mucosa to Gastric Cancer by *Ex vivo* Magnetic Resonance Spectroscopy

Carlo Calabrese,[1] Annamaria Pisi,[2] Giulio Di Febo,[1] Giuseppina Liguori,[1] Gianfranco Filippini,[2] Maurizio Cervellera,[3] Valeria Righi,[4,6] Patrizia Lucchi,[4] Adele Mucci,[6] Luisa Schenetti,[6] Valeria Tonini,[3] Maria Raffaella Tosi,[5] and Vitaliano Tugnoli[4]

[1]Dipartimento di Medicina Interna e Gastroenterologia, [2]Dipartimento di Scienze e Tecnologie Agroambientali, [3]Scienze Chirurgiche ed Anestesiologiche, and [4]Biochimica ''G. Moruzzi,'' Università di Bologna; [5]Istituto di Genetica Molecolare-CNR, Sezione di Bologna, Bologna, Italy; and [6]Dipartimento di Chimica, Università di Modena e Reggio Emilia, Modena, Italy

Abstract

Background and Aims: **The metabolic profile and morphologic aspects of normal and pathologic human gastric mucosa were studied. The aim of the present research was the application of *ex vivo* high-resolution magic angle spinning magnetic resonance spectroscopy (HR-MAS MRS) to the human gastric tissue to get information on the molecular steps involved in gastric carcinogenesis and the identification of biochemical markers useful for the development of *in vivo* MRS methodologies to diagnose gastric pathologies in clinical situations.**

Methods: **Twelve normal subjects, five with autoimmune atrophic gastritis, five with *Helicobacter pylori* infection, and five with adenocarcinoma were examined. Ten biopsies were taken during endoscopy from each patient. Specimens from carcinoma were also obtained during gastrectomy. Of the 10 biopsies, 4 were used for histologic evaluation, 4 were fixed in glutaraldehyde and processed for transmission and scanning electron microscopy, and 2 were immersed in liquid nitrogen and stored at −85°C for monodimensional and bidimensional *ex vivo* HR-MAS MRS analysis.**

Results: ***Ex vivo* HR-MAS MRS identified glycine, alanine, free choline, and triglycerides as possible molecular markers related to the human gastric mucosa differentiation toward preneoplastic and neoplastic conditions. Ultrastructural studies of autoimmune atrophic gastritis and gastric adenocarcinoma revealed lipid accumulations intracellularly and extracellularly associated with a severe prenecrotic hypoxia and mitochondria degeneration.**

Conclusions: **This is the first report of synergic applications of *ex vivo* HR-MAS MRS and electron microscopy in studying the human gastric mucosa differentiation. This research provides useful information about some molecular steps involved in gastric carcinogenesis. The biochemical data obtained on gastric pathologic tissue could represent the basis for clinical applications of *in vivo* MRS.** (Cancer Epidemiol Biomarkers Prev 2008;17(6):1386–95)

Introduction

Gastric carcinoma of the intestinal type originates from dysplastic epithelium and may also develop from gastric adenomatous polyps, representing dysplastic epithelium arising in an elevated lesion (1). The main causes of chronic atrophic gastritis and gastric atrophy are the autoimmune diseases (autoimmune atrophic gastritis) due to pernicious anemia or chronic *Helicobacter pylori* infection (2, 3).

The intestinal metaplasia may be of the enteric (grade 1), enterocolic (grade 2), or colonic (grade 3) type. Grade 3 intestinal metaplasia has traditionally been thought to be the riskiest, and the extent of atrophy and metaplasia could be a better marker for premalignancy than the mere identification of small intestinal metaplasia areas (4).

Over the years, there has been much disagreement on the identification of the different grades of dysplasia and early gastric cancer. There is still a limited knowledge on metabolic alterations occurring in dysplastic or cancer cells, despite increasing indications of the involvement of some molecular components in tumor growth and invasiveness (5). Identifying molecular patterns of the different stages of gastric mucosa by advanced molecular techniques may result in rapid and effective methods for gastric adenocarcinoma diagnosis. The impact in translating new technologies into clinical practices offers an exciting novel panorama.

MRS represents an important analytic tool, giving an accurate description of the molecular composition of human tissue. It is widely applied in biomedical research, with particular attention to molecular evaluations about diagnosis, treatment, and prognosis of human neoplasms (6, 7). The metabolic profiles, associated with healthy and malignant human tissue, can be now established through *ex vivo* high-resolution magic angle spinning magnetic resonance spectroscopy (HR-MAS MRS) done directly on human tissue specimens without any pretreatment (8-10). This technique is a powerful tool to investigate the molecular composition of

Received 10/9/07; revised 3/3/08; accepted 3/13/08.

Grant support: Italian Ministry for University, Scientific, and Technological Research.

Requests for reprints: Carlo Calabrese, Dipartimento di Medicina Interna e Gastroenterologia, Università di Bologna, Via G. Massarenti 9, 40138 Bologna, Italy. Phone: 39-051-6364191; Fax: 39-051-6364138. E-mail: carlo.calabrese2@unibo.it or Adele Mucci, Dipartimento di Chimica, Università di Modena e Reggio Emilia, Via G. Campi 183, 41100 Modena, Italy. Phone: 39-059-2055076; Fax: 39-059-373543. E-mail: mucci.adele@unimo.it

doi:10.1158/1055-9965.EPI-07-2676

human tissue, potentially bridging the *in vitro* (on human tissues extracts) and *in vivo* (directly on patients) MRS.

The aim of this study was to apply *ex vivo* HR-MAS MRS to human tissues and to have information on the molecular evolution of the gastric carcinogenesis. This datum could be the basis for the development of *in vivo* MRS methodologies to diagnose gastric pathologies in clinical situations (11). Because *ex vivo* HR-MAS magnetic resonance spectra allowed the detection of high lipid amount, especially in adenocarcinoma tissues, we have undertaken a microscopic investigation to identify and locate the lipids in the cellular and extracellular environments. The present study correlates the morphologic changes detected by transmission electron microscopy and scanning electron microscopy, with the metabolic profile of the gastric mucosa of subjects who are healthy, with autoimmune atrophic gastritis, with *H. pylori*–related gastritis, or with adenocarcinoma.

Materials and Methods

Tissue Protocols. We included 27 patients (15 men, 12 women; mean age, 56.6 ± 16.9 years): 12 normal subjects (7 men, 5 women; mean age, 53.2 ± 15.2 years), 5 with autoimmune atrophic gastritis (2 men, 3 women; mean age, 64.3 ± 17.6 years), 5 with *H. pylori* infection (4 men, 1 women; mean age, 46.2 ± 21.1 years), and 5 with adenocarcinoma (2 men, 3 women; mean age, 70.6 ± 12.9 years). Twenty-two patients underwent upper gastrointestinal endoscopy, and 5 underwent gastrectomy for adenocarcinoma. Ten biopsies (antrum or gastric body), four for histologic evaluation, four for transmission and scanning electron microscopy, and two for MRS analysis, were taken from each subject during endoscopy. The specimens (biopsies and surgical samples) in patients with gastric cancer were obtained exclusively from the carcinoma site, assuring the absence of any contaminants.

The study was approved by the local ethics committee. All patients received detailed information about the procedure, and written informed consent was obtained.

Transmission Electron Microscopy. The biopsies were fixed in 5% glutaraldehyde in 0.1 mol/L of sodium phosphate buffer (pH 7.2), postfixed in 1% osmium tetroxide in the same buffer, dehydrated, and embedded in resin. Semithin sections (2-μm thick) cut with an ultramicrotome (Reichert OM-2) were observed under a light microscope. Ultrathin sections (70-μm thick) were obtained from pathologic areas chosen by light microscopy, stained with uranyl acetate and lead citrate, and examined using Philips CM10 transmission electron microscope.

Scanning Electron Microscopy. The biopsies were fixed in 5% glutaraldehyde in 0.1 mol/L of sodium phosphate buffer (pH 7.2), critical-point dried with Emitech K 850, coated with gold palladium film with an Emitech K500 sputter coater, and observed under a Philips 515 scanning electron microscope at 9 to 14 kV.

Tissue Samples for Spectroscopic Analysis. The gastric samples were frozen in liquid nitrogen and stored at −85°C until MRS analyses. All the samples were flushed with deuterated water to eliminate the blood remaining from the surgical procedure and were inserted into a zirconia MAS rotor.

Magnetic Resonance Spectroscopy. Proton HR-MAS MRS was done with a Bruker Avance400 spectrometer equipped with a $^{1}H,^{13}C$ HR-MAS probe operating at 400.13 and 100.61 MHz. Samples were spun at 4,000 Hz, and three different types of monodimensional proton spectra were acquired at 4°C to prevent tissue degradation processes, which were found to be more evident at room temperature (8, 12-14), using the following:

(*a*) A composite pulse sequence with 1.5-s water presaturation during relaxation delay, 8-kHz spectral width, 32k data points, and 32 to 64 scans.
(*b*) A water-suppressed spin-echo Carr-Purcell-Meiboom-Gill (CPMG) sequence with 1.5-s water presaturation during relaxation delay, 1-ms echo time (τ), 360-ms total spin-spin relaxation delay ($2n\tau$), unless otherwise specified, 8-kHz spectral width, 32k data points, and 256 scans; these spectra were done to separate the contribution of resonances due to macromolecules having short spin-spin relaxation times and were acquired using a CPMG spin-echo sequence $[90^\circ - (\tau - 180^\circ - \tau)n]$, choosing τ and n to separate signals according to their different T_2; signals from macromolecules and lipids having short T_2 (or large linewidth) are attenuated, leaving only the resonances due to mobile small molecules.
(*c*) A sequence for diffusion measurements based on stimulated echo and bipolar-gradient pulses with Δ of 200 ms, eddy current delay (T_e) of 5 ms, δ of 2 × 2 ms, sine-shaped gradient with 32 G/cm followed by a 200-μs delay for gradient recovery, 8-kHz spectral width, 8k data points, and 256 scans to observe components with low diffusion rates, deriving from lipids and small proteins.

Two-dimensional $^{1}H,^{1}H$-correlation spectroscopy spectra were acquired using a standard pulse sequence (cosygpprqf), 0.5-s water presaturation during relaxation delay, 8-kHz spectral width, 4k data points, 32 scans per increment, and 256 increments. Two-dimensional $^{1}H,^{1}H$-total correlation spectroscopy spectra were acquired using a standard pulse sequence (mlevphpr), 0.5-s water presaturation during relaxation delay, 100-ms mixing (spin lock) time, 4-kHz spectral width, 4k data points, 32 scans per increment, and 128 increments. Two-dimensional $^{1}H,^{13}C$-heteronuclear single quantum coherence spectra were acquired using an echo-antiecho phase-sensitive standard pulse sequence (hsqcedetgp), 0.5-s relaxation delay, 1.725-ms evolution time, 4-kHz spectral width in f_2, 4k data points, 128 scans per increment, 17-kHz spectral width in f_1, and 256 increments. The identification of >55 metabolites was done using bidimensional spectra (8, 12-14).

Statistical Analysis. MRS data were processed using the Bruker software, applying 0.5-Hz line broadening before Fourier trasformation, and were phased, and then the baseline was corrected. The results were based on a matrix consisting of 33 spectra. The MRS data points were reduced from 32k to 8k data points. The spectral width was selected to the chemical shift range of δ 8.60 to δ 0.78 by reducing the number of data points to 1,600. The values of data points around the

water signal in the range of δ 5.03 to δ 4.69 and δ 1.34 to δ 1.29 were set to zero, at which the lactate doublet occurs. Each data set was then normalized to unit area and analyzed using the SPSS statistical package (SPSS, Inc.) to get a principal component analysis. The statistical method of principal component analysis was used to differentiate the spectra of gastritis from the healthy and neoplastic gastric mucosa. The number of principal component analyses that gave the minimal total percentage variance was considered to be the required number of principal components. The score plot of the various principal components was interpreted to reveal specific grouping and the relationship among samples.

In the present context, the eigenvalue, which represents the amount of the total test variance (%), accounted for a particular factor. However, the variance of the original data can be explained by the first few principal components, and the remaining can be ignored. In this analysis, three components with an eigenvalue of >1 were found, and they accounted for ~70% of the variance.

A plot of PC1 against PC2 and PC2 against PC3 showed the maximum data spread in two dimensions. They included those data point intensities that were most correlated with the class and values of the principal components based on data point regions. Many of the data points were significantly ($P < 0.05$) correlated with the class index.

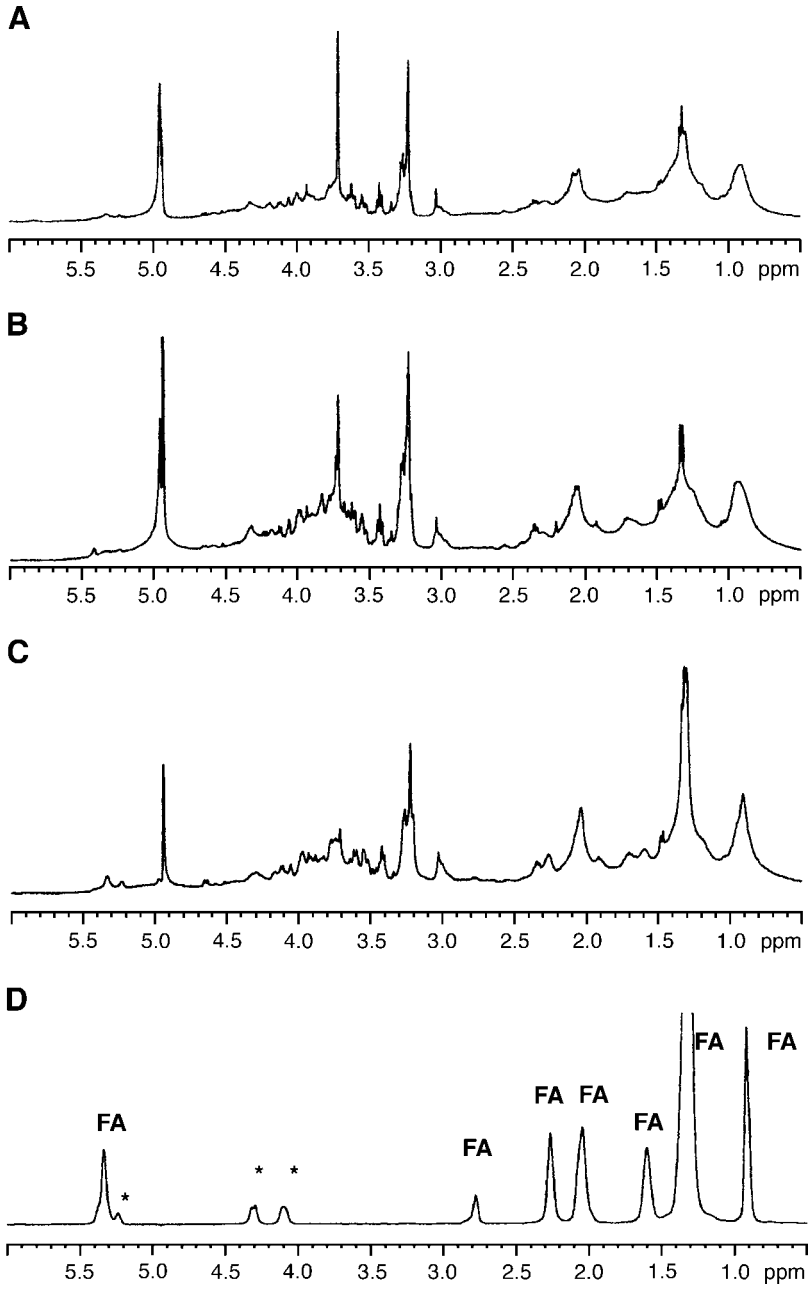

Figure 1. Proton HR-MAS magnetic resonance spectra of healthy samples (**A**), *H. pylori*–related gastritis (**B**), autoimmune atrophic gastritis (**C**), and adenocarcinoma (**D**). *, triglyceride glyceryl residues.

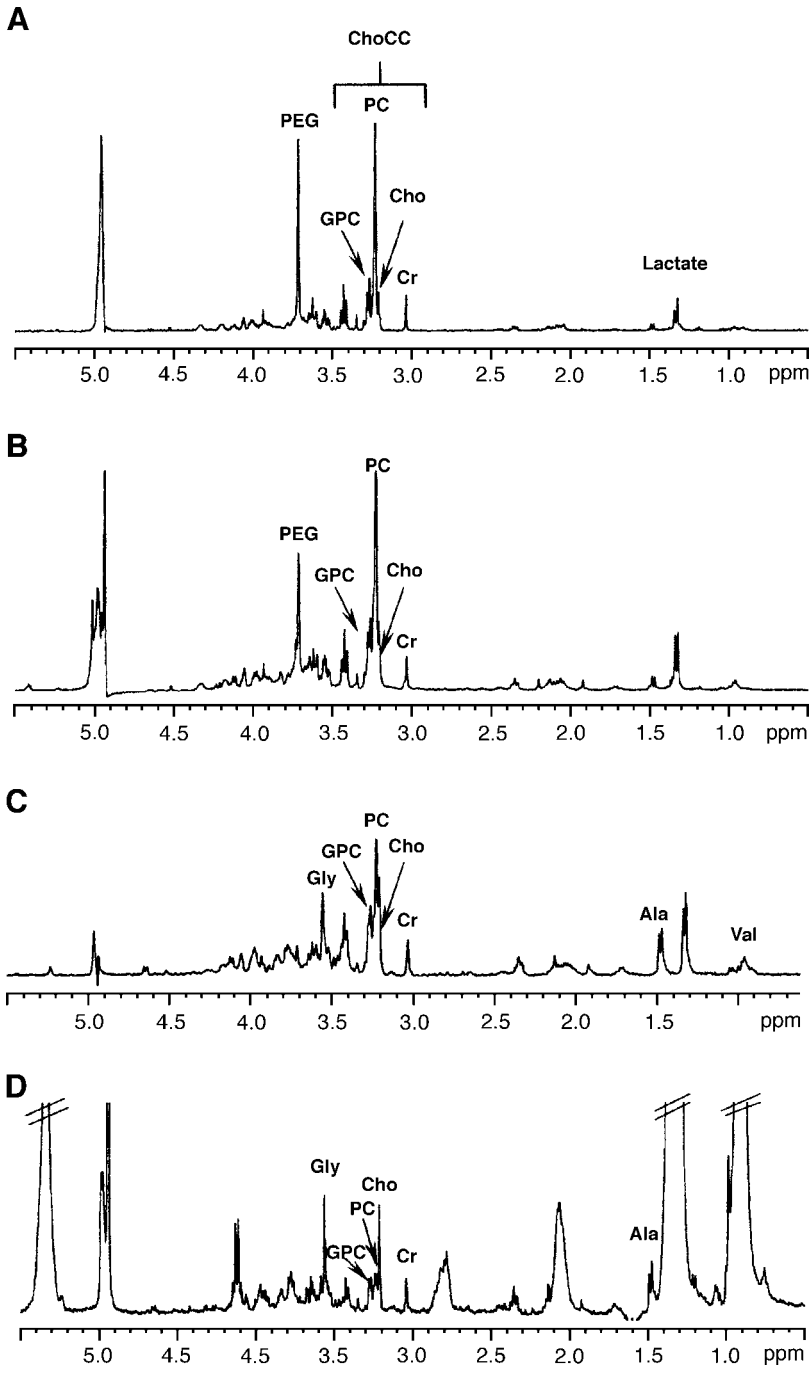

Figure 2. CPMG magnetic resonance spectra of healthy samples (**A**), *H. pylori*–related gastritis (**B**), autoimmune atrophic gastritis (**C**), and adenocarcinoma (**D**). *PEG,* polyethylene glycol.

Results

The monodimensional proton spectra of healthy mucosa, *H. pylori*–related gastritis, autoimmune atrophic gastritis, and adenocarcinoma, acquired by using a presaturation sequence with composite pulse (Bruker zgcppr), are reported in Fig. 1 (A-D, respectively). The spectra of these samples show the presence of the resonances deriving from small metabolites and macromolecules with short T_2 but not so short to be MRS invisible. The profiles of the spectra in Fig. 1A and B were quite similar, displaying broad and narrow signals. The broad signals were due to lipids and macromolecules. A progressive increase of fatty acids esterified in triglycerides passing from healthy tissue and *H. pylori*–related gastritis to autoimmune atrophic gastritis (Fig. 1C) and adenocarcinoma (Fig. 1D) was observed. In particular, the spectra of all the adenocarcinoma specimens analyzed showed the exclusive presence of triglycerides.

Spectra acquired using a CPMG spin-echo sequence showed the contribution due to mobile small molecules. The analysis of these spectra permitted a direct

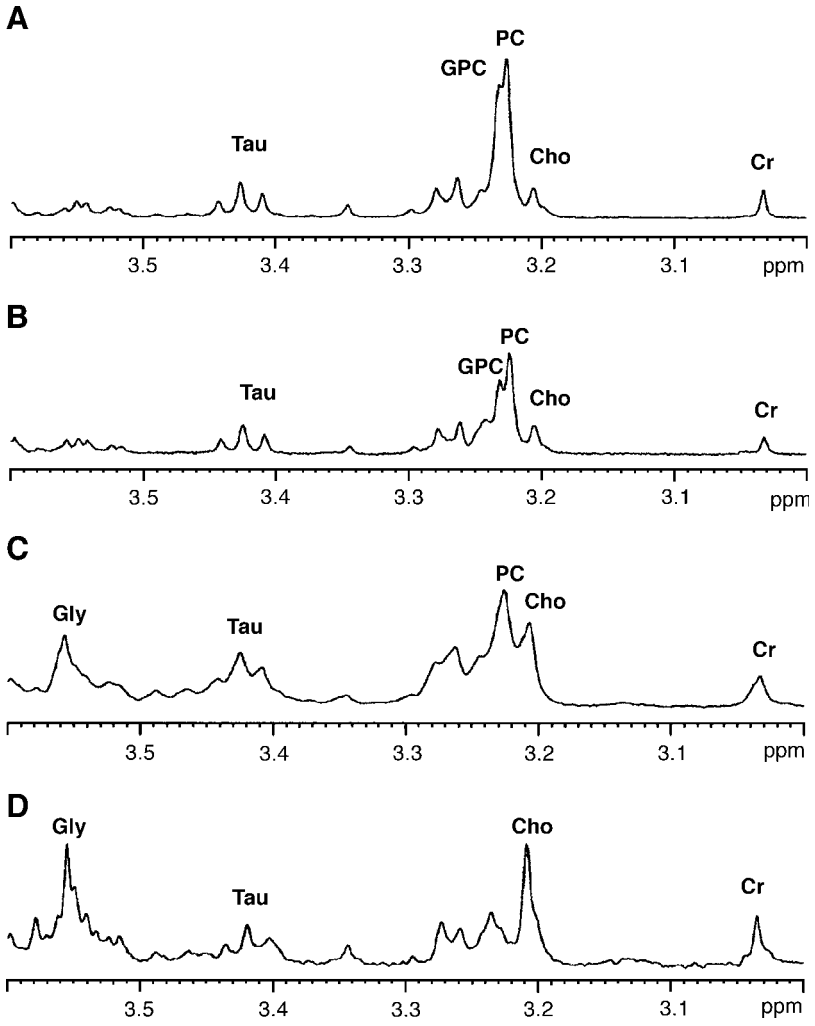

Figure 3. Enlarged region (3.6-3.0 ppm) of CPMG magnetic resonance spectra of healthy samples (**A**), *H. pylori*–related gastritis (**B**), autoimmune atrophic gastritis (**C**), and adenocarcinoma (**D**).

identification of a lot of metabolites (8, 12-14), and their differences in percentage were obtained by the inspection of CPMG spectra reported in Fig. 2A to D. The spectrum representative of *H. pylori*–related gastritis (Fig. 2B) was very similar to that of the healthy gastric mucosa (Fig. 2A). The relative concentration of choline-containing compounds and creatine measured by the ratio of choline-containing compounds to creatine and the distribution of choline-containing compounds (glycerophosphorylcholine, phosphorylcholine, and free choline) were similar. Phosphorylcholine was the most abundant in both situations. A slight increase in aliphatic amino acids, valine, leucine, isoleucine at ~1.0 ppm, and alanine at 1.48 ppm was revealed. The spectrum of autoimmune atrophic gastritis (Fig. 2C) was instead characterized by enhanced resonances due to valine and alanine. In addition, strong signals due to glycine and free choline could be detected along with the marked reduction of phosphorylcholine. The spectrum of the adenocarcinoma (Fig. 2D) displayed a dramatic increase of free choline, accompanied by very low amounts of glycerophosphorylcholine and phosphorylcholine and high amounts of glycine and alanine.

A progressive increase of free choline, glycine, and alanine, as already seen for triglycerides, was observed passing from healthy tissue and *H. pylori*–related gastritis to autoimmune atrophic gastritis and adenocarcinoma (Fig. 2). The behavior of choline-containing compounds and glycine is better shown in Fig. 3, reporting an enlarged region between 3.6 and 3.0 ppm of CPMG magnetic resonance spectra of healthy gastric mucosa (Fig. 3A), *H. pylori*–related gastritis (Fig. 3B), autoimmune atrophic gastritis (Fig. 3C), and adenocarcinoma (Fig. 3D).

Diffusion-edited spectra (Fig. 4A-D) were acquired to observe components with low diffusion rates deriving from lipids, carbohydrates, and small proteins. The profile of the spectra 4a and 4b were very similar and characterized by phospholipids, macromolecules, oligopeptides, and polysaccharides. The phospholipids were identified, in particular, by the resonances of $N^{+}(CH_3)_3$ at 3.23 ppm (^{1}H magnetic resonance spectra) and 54.8 ppm (^{13}C magnetic resonance spectra) for phosphatidylcholine (Ptd-Cho). The remaining signals arose mainly from mobile peptidic residues and polysaccharides. The peptidic residues were recognizable by the broad signals at ~4.30 ppm relative to the CH-α of bounded amino

acids by the signals at 3.0 and 1.7 ppm for lysine and at 2.30 for glutamate, and they all contributed, with phospholipids, to the signals between 1.5 and 0.8 ppm (8). The broad signals between 3.5 and 4.0 ppm and the intense signal at 2.02 ppm suggested the presence of *N*-acetylated polysaccharides referable to mucin mucopolysaccharides.

The spectrum in Fig. 4C showed an increased amount of the components due to triglycerides, signaling the molecular evolution of gastritis toward adenocarcinoma, characterized by the almost exclusive presence of triglycerides (Fig. 4D). The analysis of the spectrum showed that the triglycerides were formed by saturated, monounsaturated, and polyunsaturated fatty acids. The unsaturated acids were identified by the signals at 5.33 ppm, assigned to the ethylenic protons, and by the signals at 2.02 ppm due to the methylenic protons of the $-CH_2-CH=$ moiety of monounsaturated and polyunsaturated fatty acids.

The *ex vivo* ^{1}H HR-MAS magnetic resonance spectra (not shown) of the nine specimens collected from the margin toward the core of a large adenocarcinoma sample were all coincident and corresponded to those reported in Figs. 1D and 4D. The only detectable resonances in all of these spectra were referable to triglycerides.

The factor score plots of PC1 versus PC2 and PC2 versus PC3 showed that there were clear differences ($P < 0.05$) between adenocarcinoma and healthy samples, *H. pylori*–related gastritis, and autoimmune atrophic gastritis but not between healthy and *H. pylori*–related gastritis samples (Fig. 5).

The triglycerides, previously shown in autoimmune atrophic gastritis and adenocarcinoma samples by

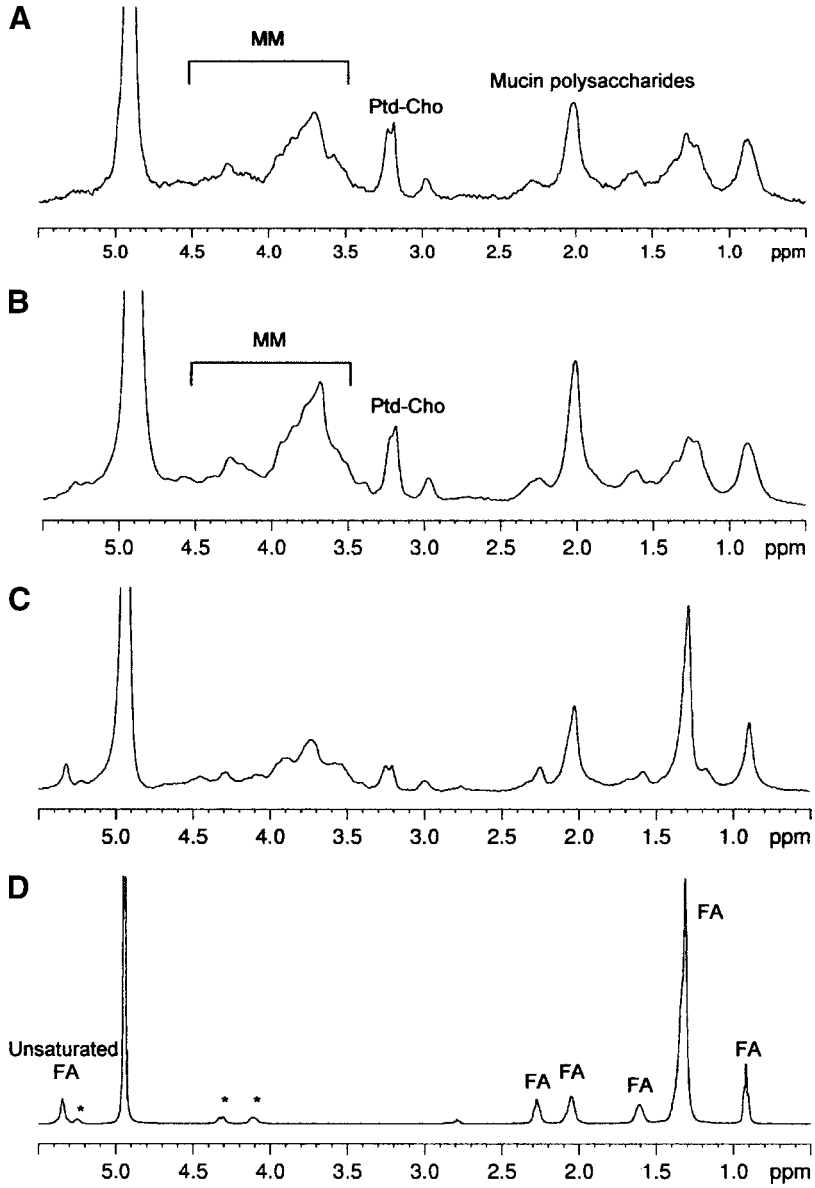

Figure 4. Diffusion-edited magnetic resonance spectra of healthy samples (**A**), *H. pylori*–related gastritis (**B**), autoimmune atrophic gastritis (**C**), and adenocarcinoma (**D**). * triglyceride glyceryl residues.

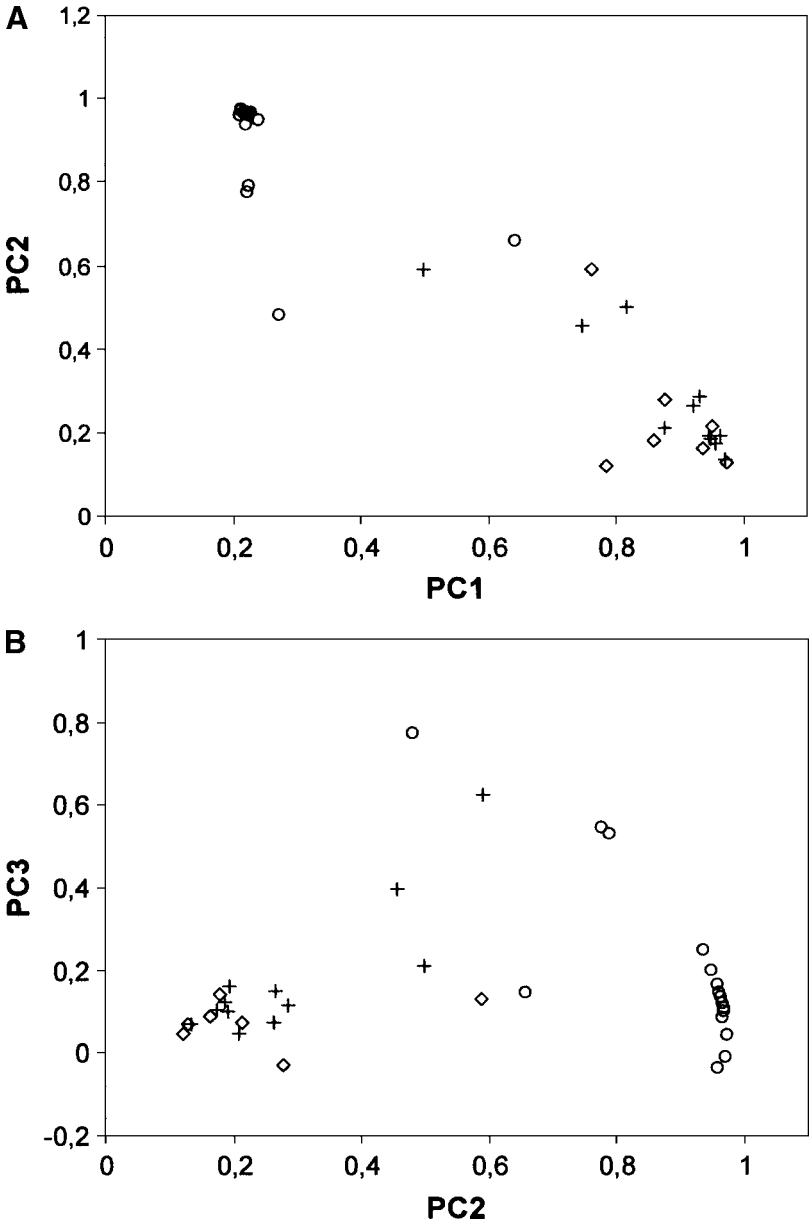

Figure 5. PC1 versus PC2 (**A**) and PC2 versus PC3 (**B**) score plots; clusters of adenocarcinoma versus healthy and *H. pylori*–related gastritis samples. ○, adenocarcinoma; ◇, *H. pylori*–related gastritis and autoimmune atrophic gastritis; +, healthy mucosa samples.

HR-MAS MRS, were detected as lipid bodies in gastric mucosa cells examined by transmission and scanning electron microscopy, but they were not visible in the light microscope. Using transmission electron microscopy, autoimmune atrophic gastritis samples showed the presence of lipid vesicles, diffuse atrophy of parietal cell mass, disappearance of cell-cell contacts, cell shrinkage, mitochondria alteration, and degradation of plasma and nuclear membranes. Using scanning electron microscopy, these lipid granules appeared quite often as grapelike shape (Fig. 6A). All adenocarcinoma specimens by light microscope showed a low-differentiated intestinal type characterized by cohesive neoplastic cells forming gland-like tubular structures in which cell cohesions were absent, and in particular, no lipid granules were detected. Using transmission electron microscopy, a large number of globular structures in the cytoplasm were seen, like those observed in the autoimmune atrophic gastritis samples. These lipid vesicles seemed well delimited and surrounded by a membrane-like layer and were mostly visible near the nuclei in most of the tumor cells (Fig. 6B). Lipid vesicles, with a diameter ranging from 0.2 to ~1.5 μm, were also revealed in tumor cells observed using scanning electron microscopy (Fig. 6C) but were not were detected in the healthy samples.

Discussion

The complex Kennedy network, characterized by biosynthetic and breakdown pathways, regulates in cells the choline phospholipid metabolism, in which more enzymes lead changes in the overall choline metabolite

profiles. Choline phospholipid metabolism was altered in a wide variety of human cancers (15). In particular, MRS studies have shown that the choline metabolite profile of tumors was characterized by an increase of phosphorylcholine and choline-containing compounds (16-18). The elevation of phosphorylcholine was mainly due to the activation of choline kinase (19, 20), which catalyzes the phosphorylation of choline for *de novo* membrane Ptd-Cho synthesis. To our knowledge, no data on the evaluation of the choline kinase expression and activity in human gastric adenocarcinomas have been published thus far (20).

Our HR-MAS MRS data showed that gastric adenocarcinomas were characterized by low levels of phosphorylcholine, free choline being the most abundant choline-containing compounds metabolite. It is likely that the high free choline amount detected in gastric adenocarcinomas is needed for the synthesis of new cell membranes in the neoplastic cells. Furthermore, *ex vivo* MRS revealed, for the first time, that a strong elevation of free choline occurs also in the autoimmune atrophic gastritis tissues when compared with *H. pylori*–related gastritis and healthy gastric mucosa. Ptd-Cho-specific phospholipase D, which catalyses the hydrolysis of Ptd-Cho to free choline and phosphatidic acid, has been implicated in cell proliferation and cancer (21). Its increased activity and expression has been reported in several human neoplasms (22-24), including gastric adenocarcinomas (25), in which Ptd-Cho-specific phospholipase D plays an important role in the promotion of cancer. This datum could explain the high level of free choline detected in the gastric adenocarcinoma samples examined. In addition, the formation of free choline and phosphatidic acid may be important in the molecular evolution of the gastric carcinogenesis because these compounds are involved in the mitogenic signaling pathway (26). Autoimmune atrophic gastritis tissue is also characterized by a high level of free choline. We then suppose that choline resonance detected in HR-MAS spectra could be the molecular signal of the gastric mucosa differentiation in autoimmune atrophic gastritis, evolving toward a preneoplastic condition. Further studies are needed to evaluate the activity and expression of the enzymatic pattern associated with the synthesis and breakdown of membrane Ptd-Cho in these tissues.

The high amount of glycine we detected in gastric adenocarcinoma has been already shown in different human tumors. For example, Griffin and Shockor (27) suggested that a preeminent glycolytic pathway in cancer cells is responsible for the glycine increase and Finch et al. (28) showed an elevation of the level of the lactic dehydrogenase in autoimmune atrophic gastritis gastric wash samples. Moreover, other authors reported a high level of glycine in glioblastomas and renal and breast tumors (29-31). Hypoxia could explain the high amount of glycine in gastric adenocarcinoma. A significant decrease in glycine was detected in hypoxia-inducible factor-1β–deficient hepatomas (32). On the other hand, it is well known that hypoxia in humans causes an up-regulation of different genes by activating the hypoxia-inducible factor-1α, which has been shown to overexpress in gastric cancer (33-35). In a similar way, a gastric cell line study showed that reactive oxygen species, produced by *H. pylori* infection, lead to an increase of hypoxia-inducible factor-1α (36).

The relative alanine concentration was another peculiarity that differentiated autoimmune atrophic gastritis and adenocarcinoma samples from the healthy and *H. pylori*–related gastritis samples. Alanine increase has been associated with different tumor types (27, 37, 38). Alanine, in conjunction with lactate, increases in tissues during hypoxia. In fact, it is formed by pyruvate transamination to prevent further increase in lactate. Ben Yoseph et al. (39) showed a strong increase of lactate

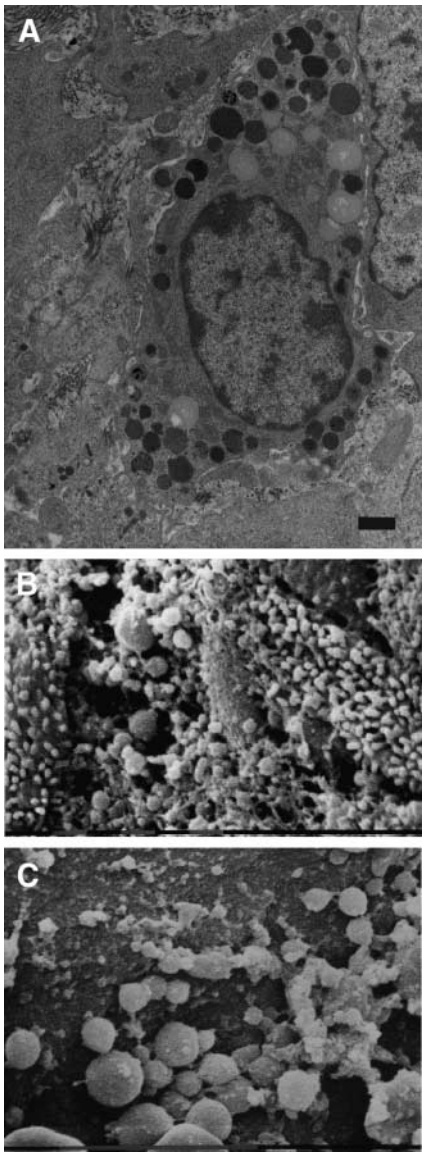

Figure 6. A. Ultrathin section of adenocarcinoma (transmission electron microscopy). Presence of intracellular electron-dense globular bodies in the cytoplasm, which could be identified as lipid bodies due to their osmiophilic nature. *Scale bar,* 0.95 μm. **B.** Autoimmune atrophic gastritis (scanning electron microscopy). Globular lipid bodies are visible singly or in clusters. *Scale bar,* 1 μm. **C.** Adenocarcinoma (scanning electron microscopy). Globular lipid bodies are visible singly or in aggregates. *Scale bar,* 10 μm.

in mild hypoxia whereas alanine increased in severe hypoxia. We hypothesize that the alanine increase in the autoimmune atrophic gastritis and adenocarcinoma samples is related to severe hypoxia conditions and could be a marker for new real-time metabolic molecular imaging for cancer diagnosis (40).

Ex vivo and *in vivo* MRS of most cancers are characterized by signals assigned to fatty acid mobile acyl chains. The appearance of mobile lipids in the spectra of intact cells is generally attributed to the formation of non–bilayer lipid structures, occurring either at the plasma membrane level or within cytoplasmic compartments (41, 42). The resonances typical of mobile lipids, identified as triglycerides, were detected in all the *ex vivo* ^{1}H HR-MAS magnetic resonance spectra relative to autoimmune atrophic gastritis and adenocarcinoma tissues, in which the distribution of the mobile lipids seemed to be homogeneous. The intracellular and extracellular lipid accumulation and mitochondria degeneration revealed by transmission and scanning electron microscopy are probably associated to a severe perinecrotic hypoxia in autoimmune atrophic gastritis and adenocarcinoma samples. Our data are supported by Goto et al. (43), who showed that the cytoplasmic accumulation of triglycerides in human fibrosarcoma cells occurred in response to hypoxic conditions and that mitochondria degeneration was probably caused by the reduction of the β-oxidation of fatty acids. A similar hypothesis was previously asserted by Freitas (44), who described lipid accumulation as a consequence of mitochondria degeneration in malignant solid tumors (45). Zoula et al. (46) correlated lipid droplets in C6 rat brain glioma to a severe prenecrotic hypoxia. We suppose that the harmful effect of the increase of free fatty acid concentration in gastric adenocarcinoma could be avoided by sequestering fatty acids as triglycerides in the form of lipid droplets.

This is the first report showing how the combined use of spectroscopic and ultrastructural methodologies could represent a powerful tool for correlating the biochemical and morphologic changes in the human gastric mucosa.

In conclusion, *ex vivo* HR-MAS MRS has been shown to be feasible even for small endoscopic biopsies and to allow the identification of free choline, glycine, alanine, and triglycerides as the possible biochemical mediators for human gastric mucosa differentiation toward neoplastic conditions. Further studies on the enzymatic pathways, on the basis of the production of these metabolites, will be useful. Moreover, the biochemical information obtained on gastric pathologic tissue could represent the basis for the clinical applications of *in vivo* MRS, which reliability is based on the identification of molecular markers.

Disclosure of Potential Conflicts of Interest

No potential conflicts of interest were disclosed.

Acknowledgments

The costs of publication of this article were defrayed in part by the payment of page charges. This article must therefore be hereby marked *advertisement* in accordance with 18 U.S.C. Section 1734 solely to indicate this fact.

We thank the Fondazione Cassa di Risparmio of Modena for the acquisition of the Bruker Avance400 Spectrometer; the Centro Interdipartimentale Grandi Strumenti of the University of Modena and Reggio Emilia; and Dr. Kent McDonald of Robert D. Ogg Electron Microscope Laboratory, University of California, Berkeley, for the technical and scientific assistance in transmission electron microscopy.

References

1. Correa P. A human model for gastric carcinogenesis. Cancer Res 1988;48:3554–60.
2. Helicobacter and Cancer Collaborative Group. Gastric cancer and *Helicobacter pylori*: a combined analysis of 12 case control studies nested within prospective cohorts. Gut 2001;49:347–53.
3. Meining A, Bayerdorffer E, Muller P, et al. Gastric carcinoma risk index in patients infected with *Helicobacter pylori*. Virchows Arch 1998;432:311–4.
4. Correa P. Chronic gastritis: a clinic-pathological classification. Am J Gastroenterol 1988;83:504–9.
5. Ferretti A, Knijn A, Iorio E, et al. Biophysical and structural characterization of ^{1}H-NMR-detectable mobile lipid domains in NIH-3T3 fibroblasts. Biochim Biophys Acta 1999;1438:329–48.
6. Nuclear magnetic resonance spectroscopy in the study of neoplastic tissue. In: Tosi R, Tugnoli V, editors. New York: Nova Science Publishers, Inc.; 2005.
7. Gillies RJ, Morse DL. *In vivo* magnetic resonance spectroscopy in cancer. Annu Rew Biomed Eng 2005;7:287–326.
8. Tugnoli V, Schenetti L, Mucci A, et al. *Ex vivo* HR-MAS MRS of human meningiomas: a comparison with *in vivo* 1H MR spectra. Int J Mol Med 2006;18:859–69.
9. Celda B, Monleon D, Martinez-Bisbal MC, et al. MRS as endogenous molecular imaging for brain and prostate tumor: FP6 project ''e TUMOR''. Adv Exp Med Biol 2006;587:285–302.
10. Lyng H, Sitter B, Bathen TF, et al. Metabolic mapping by use of high-resolution magic angle spinning ^{1}H MR spectroscopy for assessment of apoptosis in cervical carcinomas. BMC Cancer 2007;17:7–11.
11. Mun CW, Cho JY, Shin WJ, et al. *Ex vivo* proton MR spectroscopy (^{1}H-MRS) for evaluation of human gastric carcinoma. Magn Reson Imaging 2004;22:861–70.
12. Tugnoli V, Mucci A, Schenetti L, et al. Molecular characterization of human gastric mucosa by HR-MAS magnetic resonance spectroscopy. Int J Mol Med 2004;14:1065–71.
13. Tugnoli V, Mucci A, Schenetti L, et al. *Ex vivo* HR-MAS magnetic resonance spectroscopy of human gastric adenocarcinomas: a comparison with healthy gastric mucosa. Oncol Rep 2006;16:543–54.
14. Schenetti L, Mucci A, Parenti F, et al. HR-MAS MMR spectroscopy in the characterization of human tissues: application to healthy gastric mucosa. Concepts Magn Reson 2006;28A:430–43.
15. Podo F. Tumour phospholipid metabolism. NMR Biomed 1999;12: 413–39.
16. Glunde K, Jie C, Bhujwalla ZM. Molecular causes of the aberrant choline phospholipid metabolism in breast cancer. Cancer Res 2004; 64:4270–6.
17. Iorio E, Mezzanzanica D, Alberti P, et al. Alterations of choline phospholipid metabolism in ovarian tumor progression. Cancer Res 2005;65:9369–76.
18. Glunde K, Ackerstaff E, Mori N, Jacobs MA, Bhujwalla ZM. Choline phospholipids metabolism in cancer: consequences for molecular pharmaceutical interventions. Mol Pharm 2006;3:496–506.
19. Janardhan S, Srivani P, Sastry GN. Choline kinase: an important target for cancer. Curr Med Chem 2006;13:1169–86.
20. Ramírez de Molina A, Gallego-Ortega D, Sarmentero-Estrada J, et al. Choline kinase as a link connecting phospholipid metabolism and cell cycle regulation: implications in cancer therapy. Int J Biochem Cell Biol. In press 2008.
21. Foster DA, Xu L. Phospholipase D in cell proliferation and cancer. Mol Canc Res 2003;1:798–800.
22. Noh DY, Ahn SJ, Lee RA, et al. Overexpression of phospholipase D1 in human breast cancer tissue. Cancer Lett 2000;161:207–14.
23. Uchida N, Okamura S, Nagamachi Y, Yamashita S. Increased phospholipase D activity in human breast cancer. J Cancer Res Clin Oncol 1997;123:280–5.
24. Zhao Y, Ehara H, Akao Y, et al. Increased activity and intranuclear expression of phospholipase D2 in human renal cancer. Biochem Biophys Res Commun 2000;278:140–3.
25. Uchida N, Okamura S, Kuwano H. Phospholipase D activity in human gastric carcinoma. Anticancer Res 1999;19:671–5.
26. Rodriguez-Gonzalez A, Ramirez de Molina A, Benitez-Rajal J, Lacal JC. Phospholipase D and choline kinase: their role in cancer development and their potential as drug target. Progress in Cell Cycle Res 2003;5:191–201.

27. Griffin JL, Shockor JP. Metabolic profiles of cancer cells. Nat Rev Cancer 2004;4:551–61.
28. Finch PJ, Ryan FP, Rogers K, Holt S. Gastric enzymes as a screening test for gastric cancer. Gut 1987;28:319–22.
29. Lehnardt FG, Bock C, Rohn G, Ernestus RI, Hoehn M. Metabolic differences between primary and recurrent human brain tumors: a ^{1}H NMR spectroscopic investigation. NMR Biomed 2005;18: 371–82.
30. Tate AR, Foxall PJD, Holmes E, Moka D, Spraul M, Nicholson JK. Distinction between normal and renal cell carcinoma kidney cortical biopsy samples using pattern recognition of ^{1}H magic angle spinning (MAS) NMR spectra. NMR Biomed 2000;13:64–71.
31. Sitter B, Lundgren S, Bathen Tone F, Halgunset J, Fjosne HE, Gribbestadt IS. Comparison of HR MAS MR spectroscopic profiles of breast cancer tissue with clinical parameters. NMR Biomed 2006;19: 30–40.
32. Griffiths JR, McSheehy PMJ, Robinson SP, et al. Metabolic changes detected by *in vivo* magnetic resonance studies of HEPA-1 wild-type tumors and tumors deficient in hypoxia-inducible factor-1b (HIF-1b): evidence of an anabolic role for the HIF-1 pathway. Cancer Res 2002; 62:688–95.
33. Mizokami K, Kakeji Y, Oda S, et al. Clinicopathologic significance of hypoxia-inducible factor 1α overexpression in gastric carcinomas. J Surg Oncol 2006;94:149–54.
34. Griffiths EA, Pritchard SA, Valentine HR, et al. Hypoxia-inducible factor-1α expression in the gastric carcinogenesis sequence and its prognostic role in gastric and gastro-oesophageal adenocarcinomas. Br J Cancer 2007;96:95–103.
35. Zhong H, De Marzo AM, Laughner E, et al. Overexpression of hypoxia-inducible factor 1α in common human cancers and their metastases. Cancer Res 1999;59:5830–5.
36. Park JH, Kim TY, Jong HS, et al. Gastric epithelial reactive oxygen species prevent normoxic degradation of hypoxia-inducible factor-1α in gastric cancer cells. Clin Cancer Res 2003;9:433–40.
37. Tosi MR, Fini G, Tinti A, Reggiani A, Tugnoli V. Molecular characterization of human healthy and neoplastic cerebral and renal tissues by *in vitro* 1H NMR spectroscopy [review]. Int J Mol Med 2002;9:299–310.
38. Bourne RM, Stanwell P, Stretch JR, et al. *In vivo* and *ex vivo* proton MR spectroscopy of primary and secondary melanoma. Eur J Radiol 2005;53:506–13.
39. Ben Yoseph O, Baddar-Goffer RS, Morris PG, Bachelard HS. Glycerol 3-phosphate and lactate as indicators of the cerebral cytoplasmic redox state in severe and mild hypoxia respectively: a carbon-13 and phosphorus-31 NMR study. Biochem J 1993;291:915–9.
40. Golman K, In't Zandt R, Thaning M. Real-time metabolic imaging. Proc Natl Acad Sci U S A 2006;103:11270–5.
41. Iorio E, Di Vito M, Spadaro F, et al. Triacsin C inhibits the formation of ^{1}H NMR-visible mobile lipids and lipid bodies in HuT 78 apoptotic cells. Biochim Biophys Acta 2003;1634:1–14.
42. Hakumaki JM, Kauppinen RA. 1H NMR visible lipids in the life and death of cells. Trends Biochem Sci 2000;25:357–62.
43. Goto K, Asai T, Hara S, et al. Enhanced antitumor activity of xanthohumol, a diacylglycerol acyltransferase inhibitor, under hypoxia. Cancer Lett 2005;219:215–22.
44. Freitas I. Lipid accumulation: the common feature to photosensitizer-retaining normal and malignant tissues. J Photochem Photobiol B 1990;7:359–61.
45. Freitas I, Bono B, Bertone V, et al. Characterization of the metabolism of perinecrotic cells in solid tumors by enzyme histochemistry. Anticancer Res 1996;16:1491–502.
46. Zoula S, Herigault G, Ziegler A, Farion R, Decorps M, Remy C. Correlation between the occurrence of 1H-MRS lipid signal, necrosis and lipid droplets during C6 rat glioma development. NMR Biomed 2003;16:199–212.